Raspberry Pi Reflector (RPR): a Low-cost Water-level Monitoring System based on GNSS Interferometric Reflectometry

Makan A. Karegar[1*], Jürgen Kusche[1], Felipe Geremia-Nievinski[2], Kristine M. Larson[1,3]

[1] Institute of Geodesy and Geoinformation, University of Bonn, Bonn, Germany
[2]Department of Geodesy and Postgraduate Program in Remote Sensing, Federal University of Rio Grande do Sul, Porto Alegre, Brazil
[3]Aerospace Engineering Sciences, University of Colorado, Boulder, USA

[*]Corresponding author: Makan A. Karegar (karegar@uni-bonn.de)

Key Points:

- We present a prototype for tracking water levels called the Raspberry Pi Reflector with centimeter level accuracy
- It consists of cost-effective single-frequency Global Positioning System module and navigation antenna connected to Raspberry Pi microcomputer
- It uses Interferometric Reflectometry technique and can be operated safely in extreme weather with lower operational costs

This article has been accepted for publication and undergone full peer review but has not been through the copyediting, typesetting, pagination and proofreading process, which may lead to differences between this version and the Version of Record. Please cite this article as doi: 10.1029/2021WR031713.

Abstract

Although reflectometry is not the primary application of GPS and similar Global Navigation Satellite Systems (GNSS), fast-growing GNSS tracking networks has led to the emergence of GNSS interferometric reflectometry technique for monitoring surface changes such as water level. However, scientific-grade or geodetic GNSS instruments are expensive, which is a limiting factor for their prompt and more widespread deployment as a dedicated environmental sensor. We present a prototype called Raspberry Pi Reflector (RPR) that includes a low-cost and low-maintenance single-frequency GPS module and a navigation antenna connected to an inexpensive Raspberry Pi microcomputer. A unit has been successfully operating for almost two years since March 2020 in Wesel (Germany) next to the Rhine river. Sub-daily and daily water levels are retrieved using spectral analysis of reflection data. The river level measurements from RPR are compared with a co-located river gauge. We find an RMSE of 7.6 cm in sub-daily estimates and 6 cm in daily means of river level. In August 2021, we changed the antenna orientation from upright to sideways facing the river. The RMSE reduced to 3 cm (sub-daily) and 1.5 cm (daily) with the new orientation. While satellite radar altimetry techniques have been utilized to monitor water levels with global coverage, their measurements are associated with moderate uncertainties and temporal resolution. Therefore, such low-cost and high-precision instruments can be paired with satellite data for calibrating, validating and modeling purposes. These instruments are financially (< US$ 150 as of November, 2021) and technically accessible worldwide.

1 Introduction

One of the challenges for hydrologists and environmental scientists is the need to obtain and sustain *in-situ* water level measurements for calibrating and improving forecast models, validating satellite and airborne data products, and developing early-warning flood systems. Ground-based measurements are still scarce in many regions. In particular, stream flow monitoring gauges have been declining sharply since the mid 1980s due to high maintenance cost, funding shortfalls and (geo-) political constraints (Hannah et al., 2011; Ruhi et al., 2016, 2018; Reid et al., 2019). While satellite remote sensing techniques have been utilized to monitor oceanic and land surface water with unprecedented global coverage, their measurements are associated with moderate uncertainties and temporal resolution (> 7-day return) (Jarihani et al., 2013; Escudier et al., 2017). The upcoming NASA's Surface Water Ocean Topography (SWOT) satellite mission will collect high-accuracy measurements of inland surface water elevation (10 cm error for 1 km^2 areas) at unprecedented scales (10 m to 70 m resolution) using Ka-band interferometric synthetic aperture radar. SWOT will provide global maps of water surface elevation, slope and inundated areas for rivers wider than 100 m (Biancamaria et al., 2016). The SWOT interferometric swath will pass over a given location two or three times every 21-day orbital cycle (Tuozzolo et al., 2019). However, the coarse temporal resolution of satellite

altimetry missions such as SWOT and the requirement for monitoring smaller rivers and tributaries underline the significance of *in-situ* monitoring sites. Measurements of sea surface and river water level using ground-based sensors conventionally rely on contact methods, such as traditional float and stilling well gauges (Noye, 1974) and bubbler pressure gauges (Pugh, 1972), or proximal sensing gauges, such as acoustic (Gill & Mero, 1990; Boon & Brubaker, 2008), radar (Woodworth & Smith, 2003; Costa et al., 2006) and camera (Chandler et al., 2002; Kim et al., 2011; Eltner et al., 2018) sensors. The commercial versions of these sensors may be costly, ranging from few hundreds (e.g., pressure gauge) to a few thousands of U.S. dollars (e.g., radar sensors). Their installations are often restricted to a specific structure close to the river or sea such as a stilling well, a mast or a bridge, where they may be exposed to vandalism or theft. However, marked improvements in communication technology, open-source hardware, microcontrollers and single-board computers such as Internet-of-Things, Raspberry Pi computers, and Global Positioning System (GPS) chipsets are transforming scientific data collection, offering a new way forward for using low-cost sensors for environmental monitoring.

Open-source do-it-yourself sensors can vastly reduce acquisition costs – which is a major barrier for collecting *in-situ* water level data. In recent years, the use of inexpensive sensors has gained popularity in surface water monitoring and has shown great promise (e.g., Mao et al., 2020; Knight et al., 2020). For example, Paul et al. (2020) developed a cost efficient lidar-based distance sensing prototype to monitor river water level (< $150 U.S. dollars) which has accuracy inversely proportional to distance, of about 1 cm for measurement distances below 10 m under operating temperatures of 10 ºC - 30 ºC. Inexpensive pressure sensors such as MS5803 have been recently combined with low-cost Arduino microcontrollers to provide sea-level data (Beddows and Mallon (2018); Lyman et al., 2020). Knight et al. (2021) showed that while these pressure sensors can resolve water elevations to 1 cm accuracy in laboratory settings, the effect of large waves during high water fluctuations and storms can significantly reduce the quality of water level measurements.

Close-range photogrammetry is another technique for measuring river water level. Inexpensive cameras are used with single-board computers, allowing cost effective solutions to water level measurements. The camera-based systems are mostly based on a single optical

camera, monitoring staff gauge but differing in image processing techniques for detecting water line on the staff and its conversion to water level. The technique is subject to poor visibility due to weather condition, ambient noise and image distortions (e.g., Lin et al., 2018; Chen et al., 2021; Kuo & Tai, 2022). Zhang et al. (2019) and Azevedo & Brás (2021) developed monitoring systems using a single infrared camera to mitigate the visibility issue and image quality. The proposed method by Zhang et al. (2019) provided comparable accuracy to the existing float-type gauges. Average accuracy of 1.8 cm for the daytime and 2.8 cm for the nighttime measurements were determined by Azevedo & Brás (2021). Marker points and recognizable structures such as buildings, concrete walls, rocks, ground control points and even the temporal texture of the changing water surface are alternative to staff gauge for detecting and obtaining water line around the monitoring area (Young et al., 2015; Leduc et al., 2018; Eltner et al., 2018). Accuracy at the centimeter level can be obtained using image processing algorithms, image classification and more recently deep learning techniques (Vanden Boomen et al., 2021; Vandaele et al., 2021). Deep learning techniques are being integrated into new computer vision technologies to develope innovative tools for river measurements (e.g., Muhadi et al., 2021; Sermet & Demir, 2022). Camera-based systems may involve the use of stereo imaging to reconstruct the three-dimensional water surface and the surrounding land topography (e.g., Li et al., 2019). However, stereo techniques are more useful for estimating flow velocity and discharge. In general, camera-based approaches have emerged as promising solutions to river level measurement. This is particularly true for small streams where the use of conventional float-type gauges and GNSS-based sensors are challenging. However, they heavily rely on computer vision techniques and image processing algorithms which are prone to the limitations of image processing, camera calibration and high variability of environmental conditions. Also, most camera-based systems require a ground marker for detecting water level. Therefore, these methods are not applicable for monitoring sea level in the open ocean, requiring a pier, wharf, or other supporting structure.

Water level can also be measured directly by means of buoys and gliders equipped with GPS, i.e. the U.S. owned and operated version of Global Navigation Satellite Systems (GNSS), and similar GNSS instruments. Using a low-cost GNSS receiver (U-blox M8T) and a patch antenna (Tallysman TW4721) on a buoy, Knight et al. (2020) designed a unit to measure sea level with Root-Mean-Square Error (RMSE) of 1.4 cm compared to a conventional tide gauge.

This Real-Time Kinematic (RTK) positioning method requires a coastal GNSS base station at a known fixed location to allow observations relative to the moving receiver on buoy. Optimal solutions for the RTK are obtained as the distance between the moving receiver and base station reduce to a couple of tens of kilometers (e.g., Rizos & Han, 2003); this is likely a significant limiting factor for adoption of this method. Penna et al. (2018) demonstrated a GNSS glider based on Precise Point Positioning (PPP), which does not require a base station. A more serious issue to these contact methods (pressure gauges and GNSS floats) concerns safety of the equipment and sustainable monitoring due to direct exposure to the water.

2 GNSS Interferometric Reflectometry for Water Level Measurements

GNSS Interferometric Reflectometry (GNSS-IR) is an emerging technique in geodesy that has shown remarkable contributions to ground-based sea and lake level monitoring (Larson et al., 2013a; Roussel et al., 2015; Strandberg et al., 2016; Geremia-Nievinski et al., 2020; Holden & Larson, 2021). Although the primary applications of GPS/GNSS are in Positioning, Navigation and Timing (PNT), the fast growth of GPS/GNSS base station networks has led to the emergence of GNSS-IR for monitoring surface changes such as sea levels and river heights. Unlike GNSS PNT applications that rely on carrier phase and pseudorange observables, GNSS-IR is based on Signal-to-Noise Ratio (SNR) data, a measure of received signal strength. The GNSS-IR operates from a moderate distance from the reflecting surface, enabling the sensor to be sheltered and protected from storm surges and flooding events.

2.1 Principles of GNSS-IR

Each GNSS comprises a constellation of 24-32 satellites in medium Earth orbit, rising and setting in the sky a few times per day. GNSS antennas receive two kinds of radio signals: strong direct signals from the GNSS satellites and weak reflected signals from the surrounding environment. Conventional GNSS positioning uses the carrier phase observables received in direct signals from multiple satellites to determine the three-dimensional position of the antenna. In contrast, the main observable of GNSS-IR is based on the constructive and destructive interference pattern resulting from the superposition between the direct and reflected satellite signals to the receiver's antenna (Figure 1a). The reflected signal always travels a longer distance than the direct signal, reaching the antenna later. For a horizontal and planar reflecting surface

(such as a river surface), this interference pattern yields periodic oscillations in each satellite track's SNR data (Figure 1b):

$$SNR = Asin(2\pi fsin(\varepsilon) + \varphi) \quad (1)$$

where A and φ are amplitude and phase of SNR data, respectively, and ϵ is satellite elevation angle with respect to the horizon. The frequency of the oscillations ($f = 2H_r/\lambda$) primarily depends on the wavelength of the carrier wave transmitted by satellites (λ, a constant which is known *a priori*) and the vertical distance between the antenna phase center and the reflecting surface (H_r), which is the unknown of interest, termed the "reflector height" (Larson et al., 2009). Although SNR data are uniformly recorded in time for each satellite, they are unevenly spaced as a function of (sine of) satellite elevation ϵ. After removing direct signal effect using a low-order polynomial fit to each satellite's SNR measurements, the Lomb-Scargle Periodogram (LSP) (Lomb, 1976; Scargle, 1982) can be computed to identify the peak frequency (Larson et al., 2009 & 2013a) using an oversampling factor. The oversampling factor is used in LSP analysis in order to ensure smaller interval of the frequency grid points allowing an improved identification of the peak frequency (VanderPlas, 2018). After scaling the LSP frequency to the unit of reflector height as $H_r = \lambda f/2$, we used an oversampling factor to produce a LSP frequency resolution of 0.005 m. To calculate the noise level, the LSP amplitudes corresponding to a selective range of scaled LSP frequencies (e.g., a region of 0-15 m) are averaged. An individual noise range for each station is often picked as the noise level is a site-specific quantity depending on environment around the reflector and reflector height (Nievinski and Larson, 2014). Then, to ensure a precise peak frequency, the SNR data with a peak-to-noise level ratio smaller than 2.7 is disregarded (Roesler & Larson, 2018). As an additional quality control, SNR data with corresponding LSP peak amplitudes smaller than 8 (volt/volt) are discarded. More details of the theoretical principles and methods underlying SNR-based GNSS-IR may be found in the literature (Nievinski & Larson, 2014; Roesler & Larson, 2018) as well as the *gnssrefl* software description (Larson, 2021).

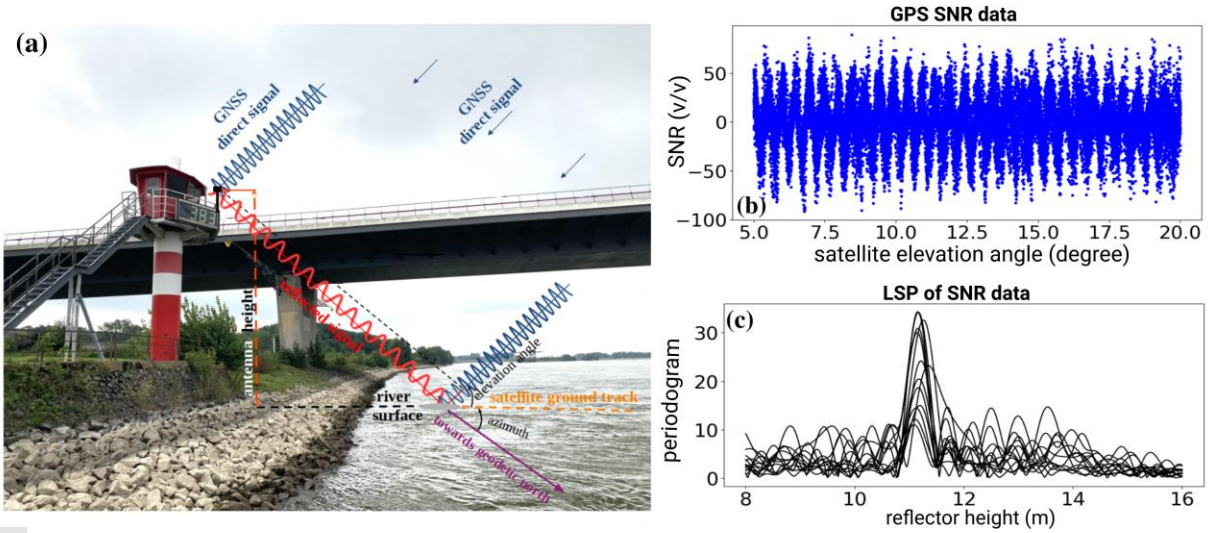

Figure 1. (a) GNSS Interferometric Reflectometry (GNSS-IR) geometry for a horizontal planar reflector. A GNSS antenna measures the interference between the direct (blue) and reflected (red) signals. Azimuth angle of the satellite is measured from the geodetic north toward the satellite ground track. The elevation angle of satellite is measured with respect to the station horizon. **(b)** Signal-to-noise ratio (SNR) data on the L1 frequency as a function of satellite elevation angle for all GPS satellite tracks (narrow ellipses in Figure 4c) facing the water (Figure 4c). These oscillation in SNR data represent the interference pattern between direct and reflected signals. **(c)** Spectral analysis of the SNR data in b). Peaks in the Lomb-Scargle Periodograms (LSP) corresponds to the estimated reflector heights for each satellite

2.2 Low-cost GNSS-IR unit

GNSS-IR is redefining its role as an innovative technique in environmental sensing. Geodetic-quality GNSS receivers and antennas, however, are still very expensive instruments (>$10,000), a limiting factor for use as a dedicated environmental sensor. While several low-cost GNSS-IR sensors are now available (see below for further details), they typically work best in coastal ocean regions and lakes where satellite signals are reflected off a relatively large extent of water body. A river is a more challenging environment for measuring water level because of the need to restrict observations over a much narrower region.

Williams et al. (2020) demonstrated the potential of a low-priced GPS receiver ($30 U.S. dollars) for tides and sea level measurements. They mounted a GPS antenna sideways on a radio tower mast at 16 m elevation in a coastal site in Ireland and collected SNR data for about three months in 2019 over a relatively large azimuth sector (140° wide). An XBee wireless telemetry system was used for short range data transfer from the mast to the computer inside the building

associated with the radio tower. Their final unit cost was ~ $500 U.S. dollars. They reported an RMS difference of 1.7 cm relative to a nearby tide gauge at daily resolution, and an RMS of 5.7 cm over a sub-daily tidal range exceeding 3 m at spring tides.

Using an upright antenna and a low-cost GPS receiver (~ $25 U.S. dollars), Fagundes et al. (2021) acquired SNR data next to the Guaíba Lake (Brazil) for approximately one year starting in 2018. They also used a large azimuth sector (180º wide) over the lake, and a relatively short antenna mount (~ 3.5 m). They reported the daily averages of water level between the GNSS-IR and a nearby gauge ~ 2.9-cm RMS level. Their unit total cost, including solar power, was ~ $200 U.S. dollars. Purnell et al. (2021) employed a stack of side-facing low-cost antenna and receivers (total cost ~ $200-300 U.S. dollars including solar panel and battery) to track the L1 frequency of multiple GNSS constellations. The water surface reflections extended more than 140º in azimuth and over a range of elevation angles up to 50º. Collecting a few weeks of SNR data at three sites along the Saint Lawrence River in Quebec (Canada) and along the Hudson River in New York (USA), they showed a RMS difference of 0.7 cm–1.2 cm with nearby tide gauges.

The initial GNSS-IR studies used a zenith-pointing geodetic antenna designed for GNSS PNT applications which suppress reflections (Larson et al., 2013b, Löfgren et al. 2014). These sites have the advantage of sharing multiple uses (i.e., positioning and reflectometry). They can also observe multiple GNSS constellations and carrier frequencies. However, besides the cost, they are not as precise as a custom-designed GNSS-IR sensor. The latter can be achieved by orienting the antenna towards the water body (generally 90 degrees from zenith; Santamaría-Gomez & Watson, 2017). Such installations have far superior reflection characteristics at the cost of poor positioning capabilities. GNSS-IR also benefits from using an inexpensive GNSS antenna which does not mitigate reflections to the same extent as larger geodetic antenna (Williams et al., 2020; Fagundes et al., 2021; Purnell et al., 2021).

Real-time GNSS observation can enable a range of opportunities for hydrological monitoring using cost-effective sensors that can be operated unattended for a long period. Thus, it is beneficial to provide real-time or near real-time transmission of data from the sensor to

remote centralized data storage and processing server. This is especially important for harsh environments or during extreme weather events such as floods, storm surges, and tsunamis when rapid response and possible evacuation is needed. In addition to remote data streaming, such telemetry capability allows a supervised remote control of GNSS unit, i.e., uploading of commands to the sensor for maintenance and upgrade. Nevertheless, because of very recent implementation of these low-cost GNSS-IR units in surface water level monitoring, there is still room for improvement, particularly with regards to telemetry, telecommand and real-time applications. Moreover, there is still a lack of information concerning their long-term performance.

We present a prototype GNSS-IR system which we have called the Raspberry Pi Reflector (RPR). It includes a low-priced and low-maintenance single-frequency GPS module and a GPS navigation antenna connected to an inexpensive Raspberry Pi computer and a cellular modem. The system enables real-time access to SNR data and orbital information and remote supervision and maintenance of GPS electronics and software. RPR builds on an earlier GNSS-IR development by adding telemetry capabilities to the offline Multipath Hardware (MPHW) sensor (Fagundes et al., 2021). A unit has been successfully operating for almost two years since March 2020 in Wesel (Germany) at a river gauge next to the Rhine river. The RPR antenna was mounted at approximately 12.5 m from the river level on a steel mast tied to the gauge building. Most of the data were collected with an antenna setup in zenith direction. To quantify the impact of antenna orientation, the antenna was mounted sideways toward the river in August 2021. Sub-daily and daily water levels are retrieved from the RPR using the *gnssrefl* Python software package (Larson, 2021). The accuracy of water level retrieval from GNSS-IR technique using RPR for this site is demonstrated by comparisons of sub-daily and daily water level retrievals with data from a classical float gauge.

2 Instrumentation

2.1 Hardware and Electronics

The RPR unit consists of two main subsystems: i) GNSS-IR sensor ii) Raspberry Pi microcomputer (Table 1 and Figure 2).

2.1.1 Legacy GNSS-IR Sensor (MPHW)

The GNSS-IR sensor is based on the successful Multipath Hardware (MPHW) implementation that Fagundes et al. (2021) designed and demonstrated to monitor lake water level. In its turn, the MPHW is based on the Free-Standing Receiver of Snow Depth (FROS-D; Adams et al., 2013). The MPHW includes a single-frequency L1 (1.575 GHz) chipset (MediaTek MT3339) mounted on an Adafruit GPS FeatherWing daughterboard, capable of tracking up to 22 satellites. MPHW also uses an external Right Hand Circular Polarized (RHCP) 28-dB Chang Hong active antenna with an Ingress Protection (IP) rating 66 enclosure which is waterproof against hose-directed water, rain or snow. The GPS board is stacked to an Adafruit Feather Adalogger mainboard based on the ATmega32u4 microcontroller. The microcontroller board is the intermediate layer between the GPS board and the Raspberry Pi microcomputer. It sends out configuration and data collection commands to the GPS board and streams the GPS data tracked by the receiver to Raspberry Pi. Both data and power are transmitted via a micro-USB cable. The MPHW GNSS-IR sensor outlined in Table 1 and Figure 2 are housed inside a IP66/67 weatherproof enclosure. The hardware outputs GPS SNR data in National Marine Electronics Association (NMEA) 0183 format (NMEA, 2018). NMEA 0183 is one of GNSS standard protocols for real-time position, velocity, time and SNR exchange with GNSS receivers. The NMEA protocol uses a plain text encoded in ASCII and contains 19 interpreted sentences for each epoch. Instructions for building the GNSS-IR sensor are provided in the supplementary information (Text S2). For the factory default Adafruit GPS FeatherWing board, SNR data are recorded with 1-dB resolution which degrades the ability to estimate reflection parameters, especially at higher elevation angles (Larson & Nievinski, 2013). We used MPHW's updated GPS firmware (Fagundes et al., 2021; Adams et al., 2013) to generate the SNR data with 0.1-dB resolution (see Text S2). Satellite azimuth and elevation angles are provided as integer values.

2.1.2 Raspberry Pi

The Raspberry Pi (Upton & Halfacree, 2014), released in 2012, is an easy-to-use, low-power, single-board tiny microcomputer that includes main input/output and Ethernet ports, and supports open source Linux-based operating systems (https://www.raspberrypi.com/software/operating-systems/). It can be used like a personal laptop as a fully functional computer, enabling storage, analysis and visualization of data with a vast

variety of third-party packages available. Open-source sensors in environmental monitoring are increasingly being built upon the Raspberry Pi (RPi) microcomputers. Raspberry Shake, a low-cost seismograph, serves as a leading example that has demonstrated the capability of RPi for long-term motioning (https://raspberryshake.org/). Some recent field applications include observing carbon dioxide concentrations (Martin et al., 2017), and ionospheric irregularities (Rodrigues & Moraes, 2019). We used RPi 4 Model B with 2 GB RAM and 64-bit quad core processor running at 1.5GHz. We used an on-board heat sink and a thermal pad which allows transferring heat between the RPi's CPU and the housing case and ensure functionality of RPi computer in outdoor summer temperature. Given the limited storage space on the RPi and real time applications, we set up an external server through SSH (Secure SHell) network protocol to communicate with the RPi microcomputer and MPHW GNSS-IR sensor. Internet connectivity can be achieved via an Ethernet/LAN cable, via Wifi or an USB dongle (cellular modem). We used an LTE dongle (Huawei E3372 4G/LTE modem) which supports a maximum rate of 150 Mb/s in download and 50 Mb/s upload and compatible with a range of operation systems such as the RPi operation system. The Huawei E3372 dongle comes with a connector for an external antenna for better signal reception from a local internet service provider, which was not used. However, we did not include this USB dongle in Table 1 as an add-on component to RPR since we consider it as an external peripheral that mainly depends on having access to this specific product.

Conventionally, Arduino-based boards provide low-power solutions for collecting environmental data. For example, the Arduino UNO microcontroller can be used with GPS module and Arduino GSM (Global System for Mobile communication) board for streaming real-time GPS data in NMEA format (Khin & Oo, 2018). The ATmega328P board is another example of low-power microcontroller that can be programmed using Arduino Integrated Development Environment (IDE) software. It was recently used together with a MS5803 pressure sensor for measuring wave height (Lyman et al., 2020). The new low-power Adafruit development board, Adafruit WICED Feather (Townsend, 2022), equipped with Arm Cortex M3 microcontroller and 128KB SRAM and WIFI chipset could be alternative to both RPi and the preceding development board (the Adafruit Feather 32u4 Adalogger) which we used in our RPR design. Adafruit WICED Feather could be mounted on the GPS module and transfer GPS data to

a data server via WIFI network. However, the RPi was chosen over these lower power microcontrollers because it allows supervised remote control of GPS module. Occasional data loss may occur during data collection due to the malfunction and failure of GPS board and/or microcontroller board as well as GSM network issues. The former issue can be solved by re-compiling and uploading the Arduino IDE sketch from the RPi to the GPS unit. For this purpose, we access the RPi desktop remotely with VNC (Virtual Network Connection) client (Text S2). Secondly, when focus is on real-time water level monitoring, RPi can operate as a cloud data server allowing real-time data transmission. Open-source client-server environments such as nextCloud can be easily installed in RPi so that it can operate as a cloud server for real-time broadcasting GPS data (Princy & Nigel, 2015). This represents a trade-off between the need for real-time water level monitoring, low-power consumption strategy when using a photovoltaic energy system and telemetry bandwidth. Thirdly, the potential to process the SNR data in the RPi and transmit only resulting water level from the on-site RPR sensor to the data server is practical when and where available telemetry bandwidth is limited. The file size of an uncompressed daily GPS data is ~ 38 MB and about 1.1 GB per month. Transferring the entire GPS observation data file may be cost prohibitive in rural locations. In contrast to Arduino and Adafruit microcontrollers, a RPi microcomputer has powerful processing capacity, so SNR data could be analyzed in RPR at the observing site to retrieve water level. The water level data are then transmitted in order to reduce telemetry needs. This is particularly important aspect where GSM signal coverage is limited and alternative low-bandwidth data communication technology such as LoRaWAN is available (data rates range from 0.3 kb/s to 50 kb/s. Lora Alliance, 2017). Fourth, RPR tracks only GPS satellites. In future cases, multi-GNSS sensors can be added to RPR to increase temporal resolution of water level retrieval. Further development may also include adding camera and flow velocity sensors to RPR for estimating and measuring discharge, respectively. RPi can easily facilitate the addition of new functionality and as a result, RPR can steadily support the addition of data records with the goal of becoming an open-source hardware maintained by the user community. More sensors mean larger data collection which could again spotlight the processing ability of RPi and on-site water level processing.

Table 1. Off-the-shelf components of the Raspberry Pi Reflector (RPR). Costs are accurate as of November 2021. The main hardware is illustrated in Figure 2. *MPN is Manufacture Product Number. [1]Note that Adafruit Feather Adalogger development board comes with a microSD card holder which is not used in the RPR unit. If available on stock, the basic development board (Adafruit Feather Basic Proto) can be used instead as it is slightly cheaper.

subsystem	component	function	version & MPN*	source	price (USD)
Raspberry Pi (RPi)	RPi	uploading commands to GPS, data transfer	4, Model B, 2GB RAM, & RASPBERRY-PI-4-2GB*	https://www.raspberrypi.org/	$35
	RPi plug-in power	power supply	15.3W USB-C & KSA-15E-051300-HU/US/WT*	https://www.raspberrypi.org/	$8
	Heat sink pack	on-board heat sink	Z-0266*	https://de.rs-online.com	$1.29
GNSS-IR sensor	Adafruit GPS FeatherWing	a single-frequency GPS L1 C/A receiver	Ultimate, MediaTek MT3339 & 3133*	https://www.adafruit.com/product/3133	$24.95
	Adafruit Feather Adalogger or Adafruit Feather Basic Proto[1]	microcontroller to interface GPS and RP	32u4 & 2795* or 2771*	https://www.adafruit.com/product/2795 or https://www.adafruit.com/product/2771	$21.95 or $ 19.95
	Chang Hong GNSS antenna	external active antenna, 3-5V and 28 dB	Chang Hong GPS-01-174-1M-0102 & 960*	https://www.adafruit.com/product/960	$17.95
	Lithium coin battery	backup power for built-in clock in GPS receiver	CR1220 12mm & 380	https://www.adafruit.com/product/380	$0.95
	Header Kit for Feather	pair GPS & microcontroller boards	12&16-pin female Header & 2886*	https://www.adafruit.com/product/2886	$ 0.95
	Fibox polycarbonate housing	IP66/67 weatherproof housing	180x130x75 mm & PCM 150/75 T*	https://de.rs-online.com/	$24
additional components	Micro SD card	disk storage for RPi	16 -128 GB, class 10	https://www.amazon.com	$8.5
	SMA to RF adapter cable	for connecting the antenna to GPS board	-	https://www.adafruit.com/product/851	$3.95
	USB to micro USB plug cable	For connecting the RPi to the microcontroller	-	https://www.amazon.com	$6.71
	Cable gland	allow cables to enter/leave the housing	M20, waterproof	https://www.amazon.com	$6.49

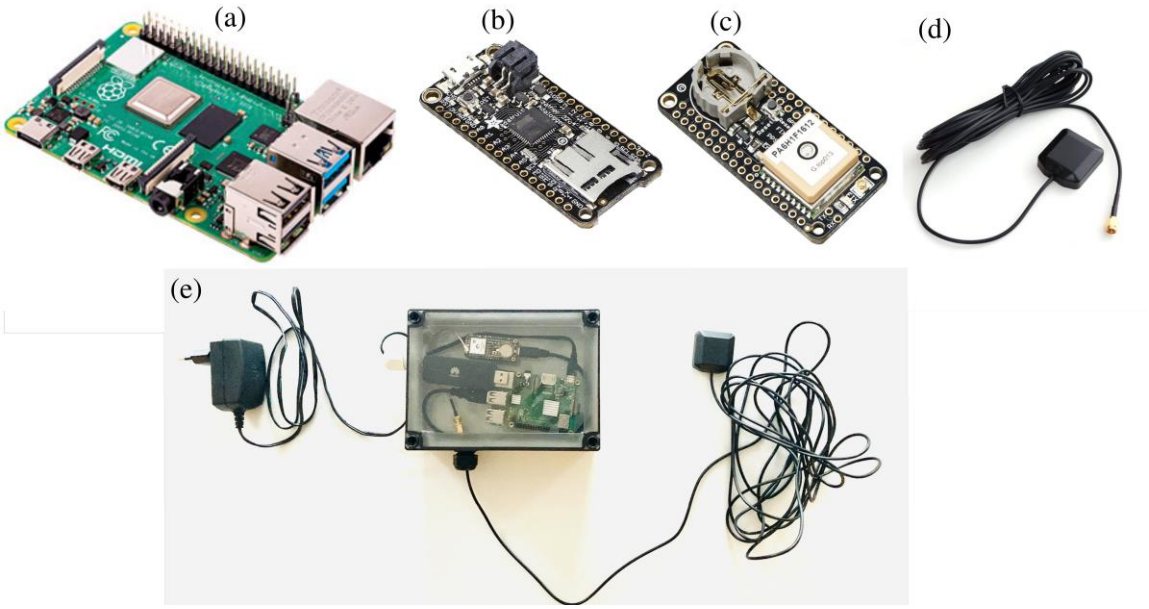

Figure 2. The RPR hardware array comprising: (a) Raspberry Pi 4 Model B (b) Adafruit Feather Adalogger microcontroller (c) Adafruit GPS FeatherWing receiver (d) GPS external antenna (e) Configuration of RPR prototype setup used. This setup uses 4G/LTE dongle modem.

The current system works with an AC/DC adapter, for particularly accessible utility power supply environments. As an alternative, the RPR can be powered using photovoltaic energy system instead of a grid power supply. We have also tested a RPR unit built based on RPi 3B+, which consumes less power than RPi 4. Details of our photovoltaic energy system architecture and power consumption measurements are given in the supplement info (Text S1). The alternative solar-powered RPR device requires only an initial site visit for installation. However, additional site visits may be required for changing the 12V battery (Figure S3) after a few years. We are using a maintenance-free cycle sealed lead acid battery with a lifetime up to 5 years. The lifetime of this kind of battery depends mainly on ambient temperature and number of cycles.

Figure 3 shows a flowchart outlining steps to set up the RPR. To configure the RPR, the RPi should be initialized based on the installation guidelines from the Raspberry Pi Foundation (https://www.raspberrypi.com/software/). Arduino IDE software is then installed on the RPi. The IDE embeds support for Adafruit boards, allowing to write, compile and upload Arduino sketches to the GPS module. Next, the GPS module is assembled. The Adafruit GPS

FeatherWing daughterboard is soldered onto the Adafruit Feather Adalogger and is then connected to the RPi. This step involves only basic soldering skill. To configure the GPS module, we have provided Arduino sketch file which is compiled and uploaded to the Adafruit boards. Finally, several Python codes are provided to initiate GPS data logging. The RPR requires 4-6 hours of unskilled labor to configure using the detailed setup instruction provided in the supplementary information (Text S2).

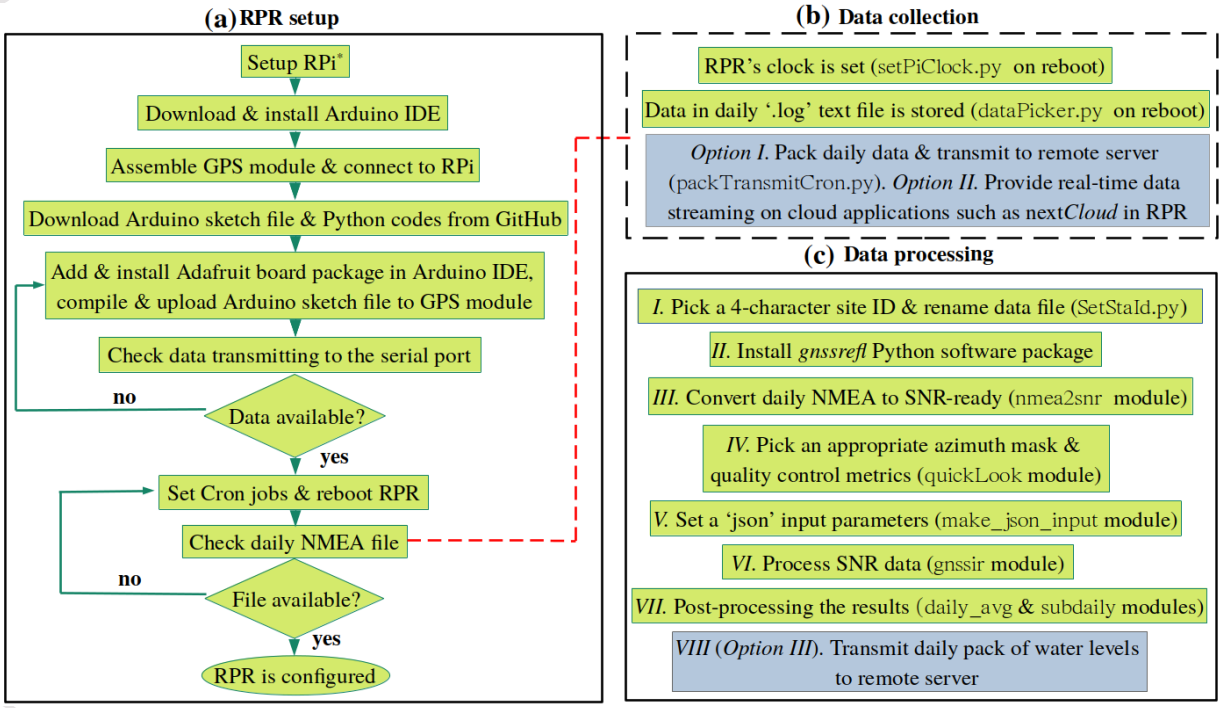

Figure 3. Flowchart of **(a)** RPR setup **(b)** data collection and **(c)** data processing. Detailed instructions for RPR setup are provided in the supplementary information (Text S2). The blue boxes indicate options for data transfer to a remote data server. *RPi is Raspberry Pi.

2.2 Software

Three layers of software programs are utilized to initialize and operate the RPR and to process collected observations. The first layer is based on the Arduino IDE, which is used to compile and upload Arduino sketches and allows to configure, set up and communicate with GPS module. The second layer is made of embedded Python codes, which initiates the RPR, enables acquiring GPS data and storing in a text file, and updates the RPR's clock. And the last layer is the *gnssrefl* open source Python software package, which is used for retrieving water level from SNR data (Larson, 2021).

2.2.1 Arduino IDE

The 32u4 microcontroller is programmed via the Arduino IDE, a simple platform based on the C/C++ language that provides a user-friendly interface. Arduino IDE enables writing, compiling and uploading programs (often called "sketches") from a personal computer (e.g., the Raspberry Pi) to the microcontroler board via a USB cable (Figure 3a and supplementary Text S2). The Arduino IDE can support third-party boards such as Adafruit's via the Additional Boards Manager URLs option (see Text S2 in supplementary information). We adopted the original MPHW Arduino sketch written by Fagundes et al. (2021) to configure the GPS sensor and print the GPS data characters (in NMEA format) via a serial event. We modified the Arduino sketch to stream only GPS data to a serial port instead of writing to an SD card to interact with the RPi via our Python codes (explained below). This sketch includes two main parts: a "Setup" and "Loop". The "Setup" part establishes serial communication between the GPS module and the RPi computer via a USB cable, configures GPS settings (e.g., GPS sampling rate) and allocates a string variable to store the encoded GPS data. The "Loop" part keeps buffering the GPS characters in a string and streams them to the serial port.

2.2.2 Embedded Python Codes

2.2.2.1. Data Collection

We provide Python code (`dataPicker.py`) to directly read each serial event from the RPi serial port and write them to a text file. We use the `pySerial` (Liechti, 2020) library to access the serial port communication in Python. The GPS NMEA 0183 strings are written and stored as data files on the RPi. The Python code `dataPicker.py` instructs the RPR to archive daily data files for batch post-processing in the *gnssrefl* software.

Unlike standard computers, the RPi microcomputer does not include a built-in real-time clock. Its clock is synchronized via WiFi or Ethernet connection and keeps its time and date by checking the internet network. However, network issues can occur, especially when using a USB dongle and thus the correct time may not be kept during a connection break. We experienced network issues from August 21 to 31, 2020 and from March 17 to 23, 2021. Since the RPi could

not synchronize its clock, the RPR data were lost. We solved this issue by providing a second embedded Python code (`setPiClock.py`) to keep the RPR clock updated using NMEA data transmitted from the GPS module.

Data collection can be automated at the RPR boot time by defining `setPiClock.py` and `dataPicker.py` in crontab tasks (see supplementary Text S2). Crontab is an internal command-line utility which is used to schedule repetitive tasks on Linux-like operating systems. After setting the cron jobs, the RPR collects data whenever it is powered on and boots up.

2.2.2.2. Data Transmission

We consider three options for data transfer considering the case for real-time water level monitoring or strategies for low-power consumption and/or low-rate (limited telemetry bandwidth) data communication. The first option is to pack (compress) daily NMEA data to a single file and transfer it to a data center for further analysis (*Option I* in Figure 3b). We provided Python code (`packTransmitCron.py`) to compress and transfer data using SSH network protocol. This strategy is useful when: (i) telemetry capacity is limited or low-rate data communication is used. Each daily compressed NMEA file occupies less than 4 MB. (ii) the RPR is powered on by photovoltaic energy system (Figure S3), thus low-energy consumption strategy should be followed. Among RPR's components, our GSM USB dongle (HUAWEI E3372) uses the highest amount of power. The USB dongle port of RPi can be set off to save power during data collection and then wakes up for a short period of time for data transfer. We have provided Python codes for controlling USB dongle's power (Section 8.4 in Text S2). These codes can be run together with `packTransmitCron.py` as cron jobs. (iii) broadcasting real-time NMEA data is not needed so the water-level can be retrieved in a data center with up to 24 hours latency.

The second option is used when streaming of NMEA data is preferred for applications such as real-time water level retrieval. The open-source suite of client-server software such as nextCloud (https://nextcloud.com/), ownCloud (https://owncloud.com/) and many others can be easily installed on the RPR and used for real-time sharing files. We provide a quick instruction for installation and configuration of nextCloud in supplementary Text S3. The real-time

broadcasting requires high speed and limitless GSM and it draws more power since the USB dongle is always active (Text S1). The third option is addressed in Section 6.

2.2.3 Processing Python Codes (*gnssrefl*)

Our RPR data are processed using the *gnssrefl* open-source Python software package (Larson, 2021). Designed specifically for ground-based GNSS-IR applications, *gnssrefl* allows for data download from global GNSS archives, format conversion, data assessment, core processing, as well as producing daily or sub-daily reflector height. It provides support for RINEX (Receiver Independent Exchange Format) versions 2.11 (Gurtner & Estey, 2007a) and 3 (Gurtner & Estey, 2007b) as well as NMEA. Manual and installation guide are available from https://github.com/kristinemlarson/gnssrefl. For completeness, we summarize processing steps (Figure 3c). First, a four-character station name should be assigned to RPR NMEA daily data (`setStaID.py`). The RPR NMEA data are then translated to an appropriate *gnssrefl* internal format (called SNR-ready files) using `nmea2snr` command in *gnssrefl*. The SNR-ready file includes satellite ID, known as "Pseudorandom Noise" (PRN) code, satellite elevation angle with respect to the station horizon, satellite azimuth angle, time stamp and SNR observations for Coarse Acquisition (C/A) code on GPS L1 frequency. *gnssrefl* analyzes all rising and setting satellite arcs from the user-defined azimuth and elevation angle range. Next, the `quickLook` tool can be used to visually test various reflection zone settings such as elevation angles, azimuths and quality control parameters, and thus to improve quality control for the reflector height retrievals produced by the core data processing module, `gnssir`. In addition to the `quickLook` utility, other tools are available online (https://gnss-reflections.org/rzones) to help the user visualize the reflection footprint near a GNSS site. Most of input parameters are then set using a wrapper around a single command `make_json_input` which makes a uniform format, referred to as a 'json' input defined in detail here (https://www.json.org/json-en.html). Once an appropriate reflection zone mask and analysis strategy were chosen, reflector heights can be estimated using the `gnssir` module. Although *gnssrefl* can analyze signals from all GNSS constellations, only GPS L1 signals are available in this study. The dominant SNR frequencies are extracted using a LSP and converted to reflector heights (see section SNR data processing for details). Additional utilities are provided to enhance post-processing reflector heights: `daily_avg` module derives daily average of reflector height and removes outliers. This

command should be used with caution when applying to fast-changing tidal river and sea level. To visualize sub-daily reflector height, `subdaily` command removes outliers, provides time series plots and prints outputs to a text file. Outlier removal is based on either a pre-defined tolerance, in which all residuals larger than the tolerance are removed, or the standard three-sigma (standard deviation) test.

3 Test Site and Data Acquisition

To assess the long-term performance of RPR and the accuracy of its water level estimates, we deployed a unit ~ 7 m from a continuously-operating water level gauge on the Rhine river in Wesel, Germany. In March 2021, the RPR antenna was mounted about 13 m above the water surface in order to maximize the reflection zone while also keeping the antenna and electronics safely above the water surface in all anticipated river levels. We fixed the antenna on a vertically oriented steel pipe and then securely tightened the pipe to the gauge house's railing (Figure 4 and Figure 1a). The RPR electronic cases were placed inside the river gauge's building for power access. The RPR collects SNR data every 1 second for all available GPS satellites and streams the data every two hours to a remote server for archiving and processing.

The river width at our test site is ~250 m during normal water level and only reduces when there is very low water during extreme drought periods. The chosen antenna height above the river surface allows sensing reflection zones with maximum dimensions of 10 m by 190 m when the satellite elevation angles range between 5º and 20º. Thus, the water surface is fully sensed from one margin to the other. However, there is a bridge to the south of the antenna which interferes with the reflected signals. We imposed an azimuth mask to limit the reflection data to the river surface next to the RPR antenna (Figure 4c). On August 20 (2021), we changed the antenna orientation setup, from zenith-pointing to sideways facing the river surface towards the selected reflection zone. We assess the effect of such modification in our data analysis.

The river gauge in Wesel, maintaining by German Federal Waterways and Shipping Administration (WSV), records water level at 15 minutes intervals. It is a classical float and stilling well gauge sitting on the river bank and connected to the water via an underground pipe. The accuracy of the river gauge records is ~3 cm. Stilling wells act as a mechanical low-pass

filter, so the hourly bands suffer some attenuation and lagging (IOC, 2006). The level of this section of the Rhine river is rainfall-dominated. Discharge is high during winter and low during summer (Figure S1a). Flooding often occurs in winter from rainfall. However, the heavy rainfall in July 2021 led to severe flooding in Western Europe including the Rhine river. A wind sensor, operated by the German Weather Service, is located in Xanten, 12.5 km from the Wesel sensors; it measures wind speed ~10 meters above the ground at hourly intervals.

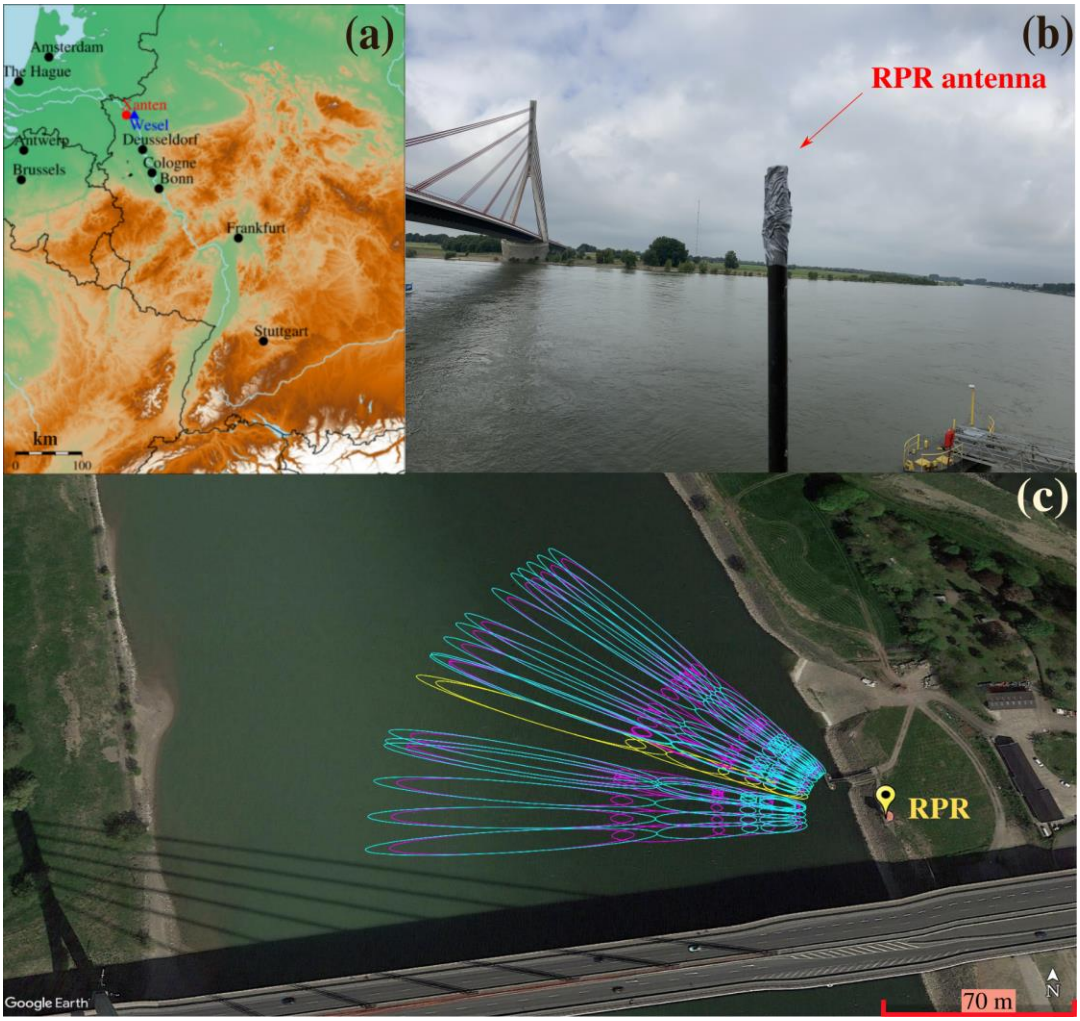

Figure 4. (a) Location and field setup of the RPR antenna in Wesel, Germany. **(b)** The GPS antenna is mounted on a steel pipe, upright-pointing from March 23 (2020) to August 20 (2021) and sideways since then. The RPR electronics are housed inside the river gauge's building (Figure 1a). **(c)** Footprints of the reflected GPS signals projected on a Google Earth image. Ellipses are reflection zones ("first Fresnel zones") corresponding to azimuth 265° - 330° and elevation 5° and 20°. Yellow ellipses refer to GPS satellite with PRN 16. Signal-to-noise ratio (SNR) data on L1 C/A data for this satellite are shown in Figure 1b.

4 SNR Data Processing

As the NMEA format is not meant for geodetic applications, satellite elevation and azimuth angles are only integer values. Since they follow a very smooth but discrete trend, the decimal parts can be restored by linear interpolation through a de-quantization process in the `nmea2snr` module of *gnssrefl.*

We imposed azimuth (265^o and 330^o) and elevation angle (5^o and 20^o) masks to isolate the reflections to the river surface (Figure 4c). The reflection footprint can be calculated by means of first Fresnel zones, the ellipses located along each satellite ground track (Larson & Nievinski, 2013). It mainly depends on reflector height and satellite azimuth and elevation (Figure 1a). In addition to the site-specific masks, the *gnssrefl* software (`make_json_input` and `gnssir` modules) also allows the user to parameterize other inputs (see section 2.1). For completeness, we summarize them here. We set the noise floor in reflector height to the region between 3 m – 16 m, we require periodogram amplitudes to be larger than 8 volts/volts (see Figure 1c), the spectral peak must be 2.7 larger than the noise, and each arc cannot last longer than 1 hour. We use a quantity called sub-daily resolution (number of satellite tracks per day) which for the RPR setup in Wesel is 9 tracks per day. We also averaged the sub-daily reflector heights (water level) over 24 hours to produce daily time series of water level (see section 5). Use cases are available on *gnssrefl* web repository (https://github.com/kristinemlarson/gnssrefl#readme) for further details.

5 Water Level Results and Discussion

The RPR instrument samples raw SNR data at 1 Hz and provides continuous and real-time SNR data via cellular telecommunication networks to a host server using nextCloud (Option II in Figure 3b and Text S3). However, the effective time required to retrieve water level for each satellite arc with GNSS-IR depends on the method used for analyzing the SNR data. Kalman filtering has been recently used to combine multiple simultaneous satellite arcs for real-time water-level retrieval (Strandberg et al., 2019). The LSP method requires, however, typically 20-60 minutes to retrieve a reflector height for an individual satellite arc. The retrieval time is site specific, depending mainly on the elevation angle mask and the vertical distance between the GNSS antenna and the reflecting surface. At our test site ~ 40 minutes on average is required for data acquisition and water level retrieval for an individual satellite track (Figure 5c).

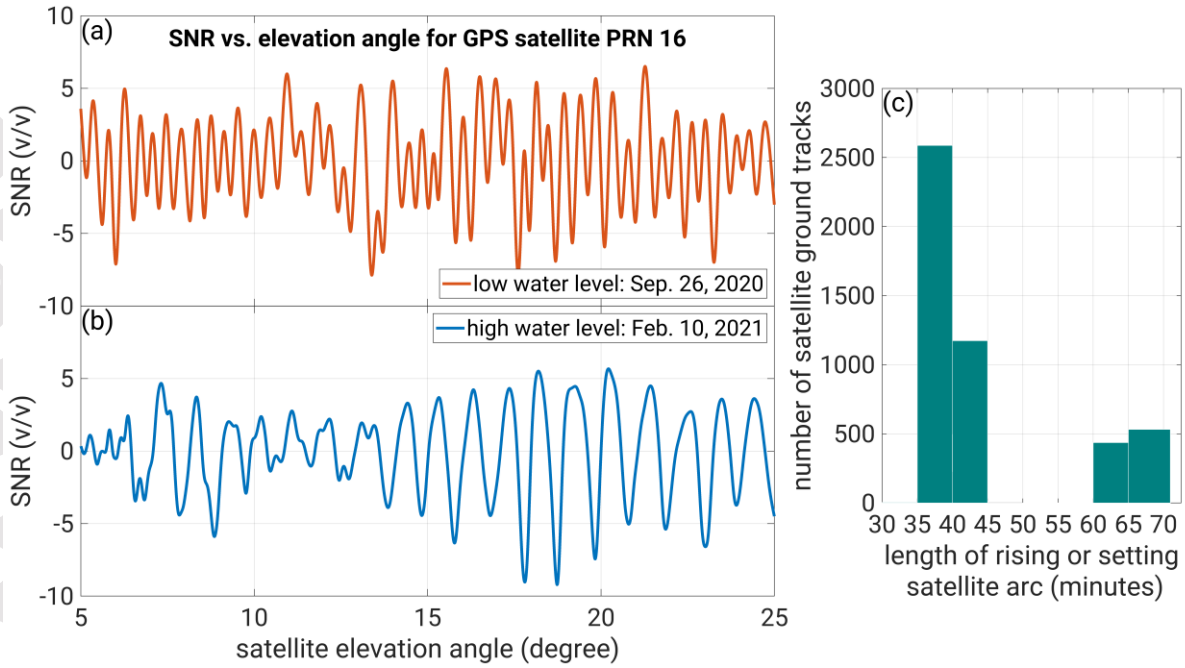

Figure 5. Detrended SNR data for the upright RPR antenna during **(a)** low river water level (1.3 m) and **(b)** high water level (9.45 m). The SNR data oscillate at a higher frequency when the reflector height is higher (red line). The 1-second SNR data were smoothed using spline interpolation. **(c)** A histogram showing time span of rising or setting satellite arc for masked elevation angles shown in Figure 4c. It takes about 30-60 minutes that signal from a given satellite is reflecting from the river surface in our test site.

Historical data (2010-2021) for the Rhine near Wesel indicates the 80th percentile of day-to-day water-level variation amounts to 20 cm (Figure S1, panels b&c). We then identified a retrieved water-level from RPR measurements as outlier when it differed from the median value of sub-daily estimates of water level by more than 20 cm. For days with sharp water fluctuations following rainfall events and spring floods, we use linear least-squares regression to find the best fit of a linear model to each RPR sub-daily water level measures. We then identified a data point as outlier when it differs from the least squares linear model fit by more than 20 cm.

Figure 6a shows sub-daily water level from RPR compared to water level from the co-located stilling well river gauge. Each RPR water level point represents an average value over the satellite descending or ascending arc. The Rhine experienced winter flooding period in mid-February followed by exceptional flood event in July 2021. Water level fluctuations during annual flooding can be substantial and reach levels of 8 m, which causes overbank flooding. The river gauge 15-minute measurements were linearly interpolated to the times of the RPR water

level estimates. The RMS of differences between two sub-daily water level time series over the entire data record is 7.6 cm. The RPR captured the diurnal variations in river level during flooding events, for example the July 2021 heavy rain induced flood event in Western Europe, as well as drought periods at low water. During July 9-16 (2021), significant rainfall sharply increased the Rhine level from 4.5 m to 8.9 m at this site. The maximum water level was observed on 16 July and then rapidly decreased. All phases of this sequence are observed accurately by the RPR. The quality of RPR sub-daily water level data is significantly improved by forming daily mean (Figure 6b). The RMS of differences between two water level data reduces from 7.6 cm (sub-daily) to 6 cm (daily). Daily averaging filters out random sources of error.

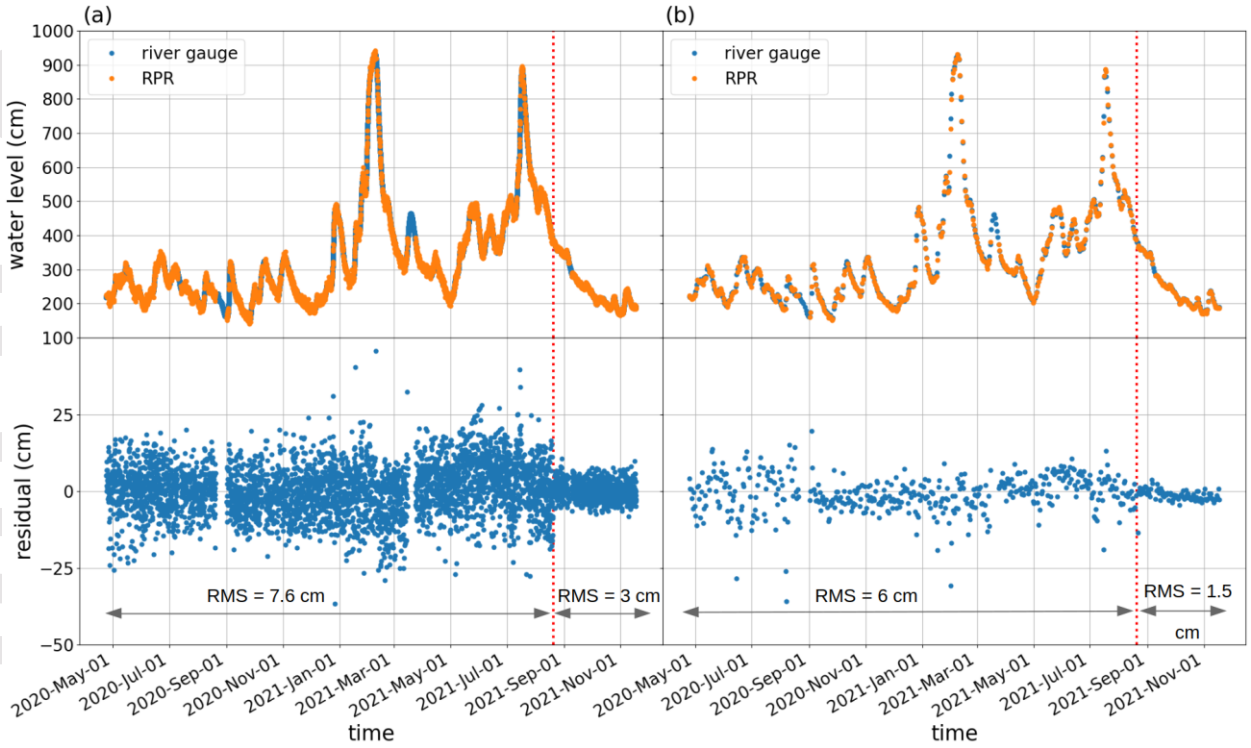

Figure 6. Water level from the river gauge and RPR. **(a)** sub-daily **(b)** daily mean. The lower panel plots are residual between the river gauge and RPR water level measurements. The vertical red dash line marks date of RPR antenna orientation change from upright to sideways. Heavy rainfall in summer 2021 (July 9-16) in Western Europe resulted in a peak at a level of about 9 m in Wesel, Germany.

5.1 Impact of Antenna Set-up Orientation

The GNSS-IR technique has primarily been used with zenith-pointing geodetic-quality GNSS instruments. Previous studies have shown that a sideways-looking antenna will improve the quality of SNR retrievals (e.g., Santamaría-Gómez & Watson, 2017). We thus set a new antenna configuration on August 20 (2021) by tilting the antenna 90^o from the vertical direction toward the river. The interference patterns recorded in SNR data from the sideways antenna are more distinct, with less noise and larger oscillation amplitudes than data from the zenith-pointing antenna (Figure 7). The increased amplitude follows from the gain applied by the antenna to surface reflections, while the reduced noise results from the mitigation of cross-channel interference when fewer satellites are tracked. For this reason, we extended the elevation angle mask up to 30^o for the new antenna setup. The improvement can be better quantified by comparing the retrieved water levels from these two datasets with the standard river gauge (Figure 6). The RMS of sub-daily residuals reduces from 7.6 cm to 3 cm for the time spans before and after the antenna orientation change, respectively. For daily residuals, the RMS decreases from 6 cm to 1.5 cm.

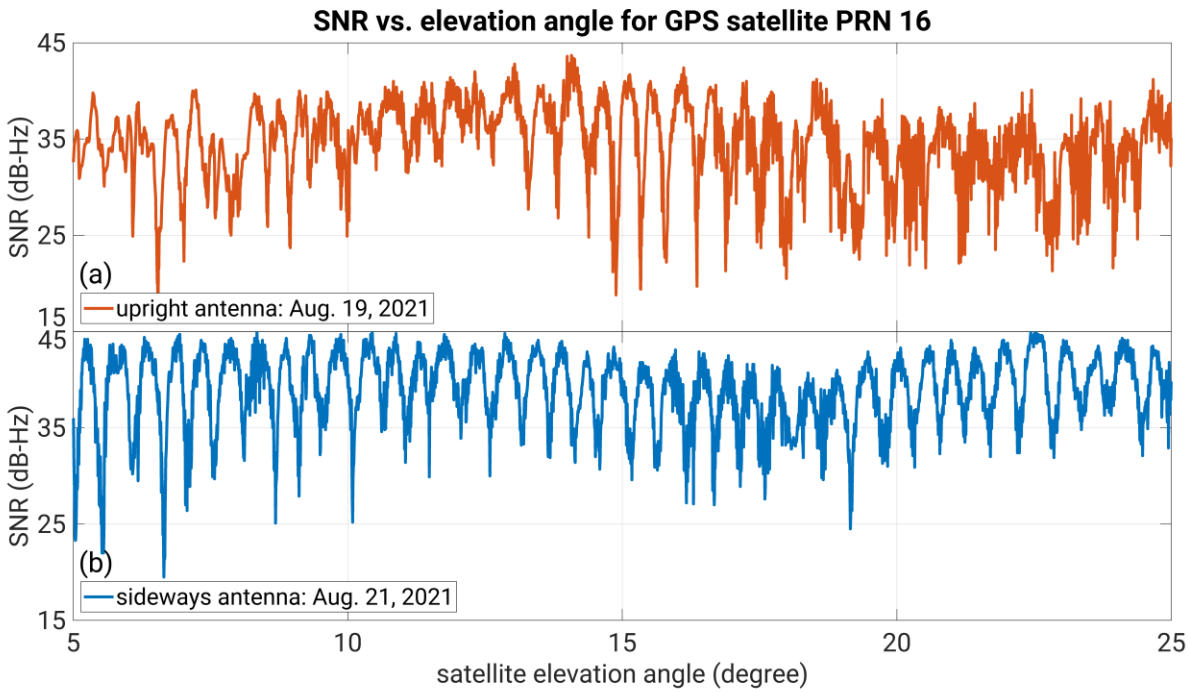

Figure 7. Examples of 1-second Signal-to-Noise Ratio (SNR) data for **(a)** upright and **(b)** sideways RPR antenna setup on August 19 and 21 (2021), respectively. The SNR data are for GPS satellite with PRN 16, (yellow ellipses in Figure 4c).

5.2 Wind Effect

The relation between the dominant SNR frequency and reflector height (GNSS-IR reflection model) is based on the assumption of the homogeneous flat and leveled reflecting surface (Larson & Nievinski, 2013). Environmental forcing such as tides, tsunami and wind introduces surface deviations, both small-scale random roughness and large-scale systematic tilting. In their turn, roughness and tilting affect respectively the amplitude and frequency of SNR oscillation, thereby decreasing the accuracy of retrieved reflector height (e.g., Karegar & Kusche, 2020; Holden & Larson, 2021). In our study area, tides are absent. To examine the possible effect of wind, we compare the differences between sub-daily RPR and river gauge time series to hourly wind speeds. Large differences are evident during elevated windy hours (> 6 m/s), when slight roughness was generated by turbulent boils on the water surface by wind (Figure 8 a&b). There is not a one-to-one correspondence between the RPR's water level uncertainty and the wind speed. For differences greater than 15 cm and wind speeds larger than 6 m/s, we found a moderate correlation ($\rho = 0.45$) (Figure 8c). However, no strong conclusive remark can be established here as the wind sensor is not co-located with our RPR and river gauge sensors in Wesel. Modification to the GNSS-IR reflection model has been suggested for sea level and significant wave height retrieval (e.g., Alonso-Arroyo et al., 2014; Roggenbuck & Reinking, 2019). However, this effect is difficult to quantify for river level, in part because smaller roughness that occurs in river surface (typically smaller than 0.3 m in height). The effect of significant wave height is more likely to be notable if the wind blows along the azimuth the antenna is pointing (Reinking et al., 2019). Residuals were reduced after the antenna orientation change. From Figure 8a&b it appears that the uncertainty from high winds is completely mitigated at this site by the sideways facing antenna orientation. As a result of this consideration, water level retrievals from an upright RPR antenna setup are more likely to be affected by wind. For sea level or tidal river applications where high tidal current speed and/or significant wave height are expected, a modification of GNSS-IR reflection model is required.

Human-induced variations have also been shown to have a large impact on accuracy of reflector height. Karegar & Kusche (2020) showed that the coherent power of a reflecting signal from a parking lot next to a GNSS site increases with beginning of COVID-19 lockdown as the reflector surface became more planar (smoother) due to absence of cars. The Rhine river is one of the world's busiest inland waterways where the high shipping traffic density itself (Figure S2) and waves induced by the busy traffic could also cause additional errors in retrieved water level.

Such a site-specific effect requires extensive screening of shipping traffic, and it could be the subject of future research.

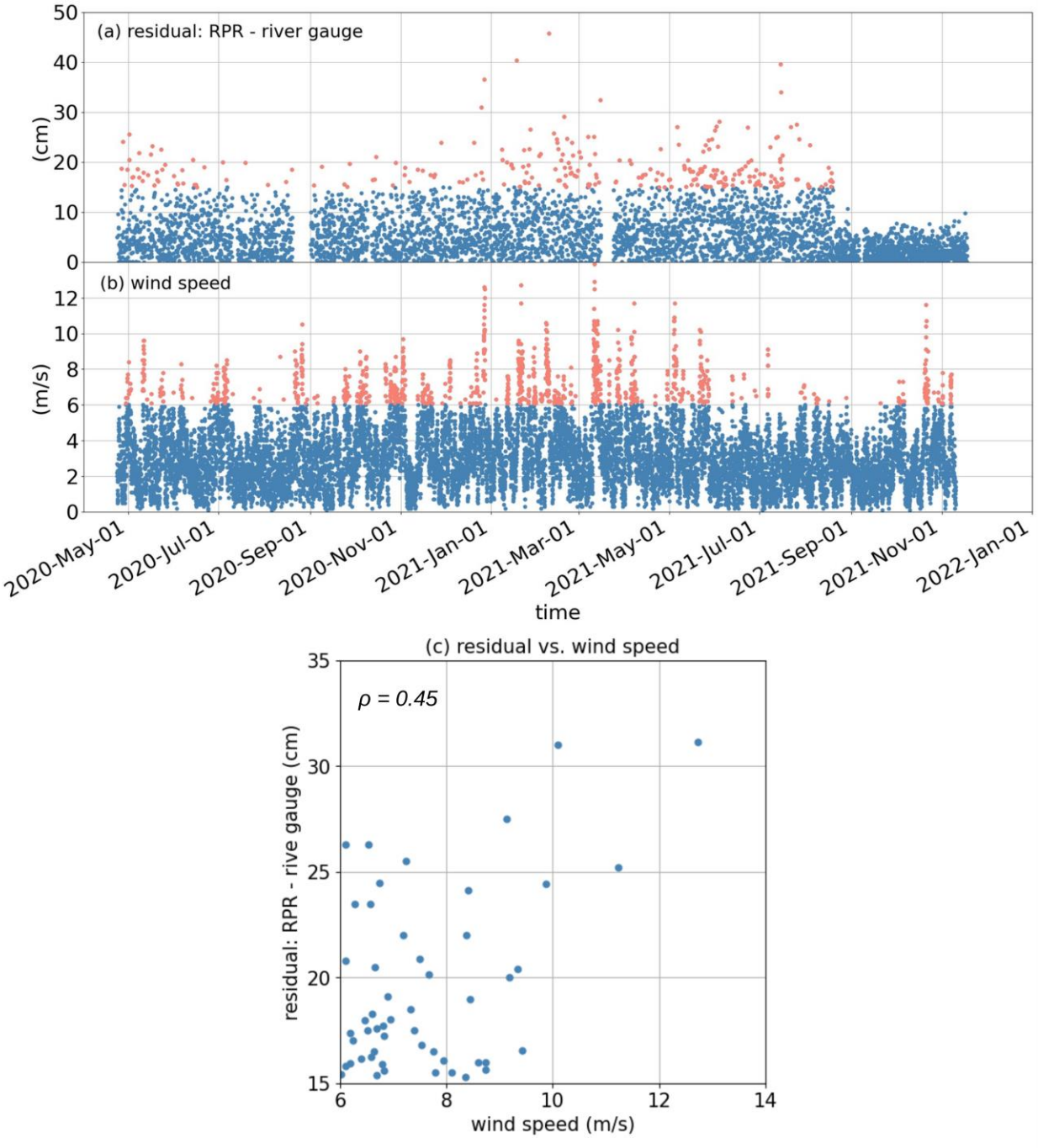

Figure 8. (a) Absolute value of water level residuals between the river gauge and RPR measurements. Residuals greater than 15 cm are shown with red dots. **(b)** Hourly wind speed measured 10 m above the ground surface at a station ~ 12.5 km from the RPR. Red dots indicate elevated windy hours larger than 6 m/s. **(c)** The relationships between water level residuals

(greater than 15 cm) and wind speed (larger than 6 m/s). The correlation coefficient (ρ) between residual and wind speed is 0.45.

5.3 Limitations

The low-cost RPR instrument has the capability of long-term monitoring of water-level and can be considered as part of adaptive monitoring efforts for maintaining the integrity of long-term water level records. However, any monitoring technique has its own limitations. First, the GNSS-IR technique has a footprint that depends on the antenna height and satellite elevation angle. For an antenna height of 1.5 m, its footprint would have an average radius of ~40 m -50 m. The footprint becomes larger as the antenna is mounted higher (e.g. ~ 200 m wide for a 13 m height at Wesel). For the GNSS-IR technique to work on smaller rivers, the antenna must be carefully placed closer to the water surface, either on the banks or in a bridge. Because of the footprint issue, it would also be necessary to rotate the antenna so that higher elevation angles could be used. Though river water level is more challenging to measure in terms of masking requirements, it could be a simpler environment in other ways because of the absence of tides.

6 Outlook for an Early-warning System

An early-warning system for hazardous events includes components of monitoring, forecasting, risk assessment, communication and preparedness (UNDRR, 2017). A river gauge network is one of the main ways of collecting, handling, analyzing and transmitting hydrological data in real time for an operational warning system. Crucially, the success of an effective drought and flood early-warning system relies on the continuous on-site measurement of precipitation, river level and flow velocity through gauge networks as detailed below. However, financial barriers challenge the sustainability of early-warning systems partly by discontinuous operations of in-situ sensors and reduced funding for maintenance, upgrade and advancements.

A basic flood warning system includes an automated local evaluation in its real-time transmission of river level data. For example, the NOAA (the National Oceanic and Atmospheric Administration) and USGS (the United States Geological Survey) developed system uses more than 10,000 river gauges to deliver near real-time data to a network of base stations where data

are processed into meaningful hydrological information (e.g., Adams, 2016; The National Weather Service (NWS), 2010). Shortly after automatic processing, data are available on a web graphical interfaces such as https://water.weather.gov/ahps/ and https://waterdata.usgs.gov/nwis/rt. The flood warnings are issued when the current water level exceeds critical thresholds. More complex flood warning systems employ physical or empirical (data-adaptive) models. Input data from river gauges are one of key components of these models (Perera et al. 2019). Typically, the physics-based models are widely used in forecasting river water level and developing flood warning system (e.g., Franchini & Lamberti, 1994; Krzysztofowicz, 2002; Vieux eta l., 2004). The European flood alert system uses the LISFLOOD hydrological model driven by meteorological forcing data to provide river flooding forecasts up to 10 days in advance (Smith et al. 2016). This hydrological model is calibrated against historical records of river discharges, and then a number of forecast products including but not limited to flood alerts are derived. At a given river gauge, the forecasts are post-processed to minimize errors in the size and magnitude of events when compared to the observed values, as well as to derive more accurate calibrated probabilistic forecasts.

For coastal flood hazard assessment, hydrodynamic models should be calibrated and validated against observed water level at river gauges. For example, Jafarzadegan et al. (2022) proposed using a digital elevation model based approach for the rapid real-time assessment of flood hazard in coastal areas. A two-dimensional hydrodynamic model is first calibrated based on observed water levels at USGS gauges and then the calibrated model is used to generate a flood inundation map for further analysis. The gauge-based (on-site) flood warning systems are regaining their popularity with recent developing of data-adaptive methods. Data-driven flood warning systems can simplify the complexity of hydrological processes while reaching high accuracy with low computational expense. These models need to be trained with river gauge data using artificial neural network and other machine learning techniques (e.g., Yaseen et al. 2015; Li et al., 2021). One such recent example is the early-warning system developed for one of the urban watersheds in Houston, USA. Using 2010-2019 data records from river and rain gauges as training and validating datasets, the model provides 30-minutes forecast of river water level (Sanders et al., 2022).

Drought indices have been developed to be used in early-warning systems. Most of drought early-warning systems focus on precipitation deficits, in part due to near-real-time data availability of global precipitation data. However, droughts are often indicated by deficits in other components of the hydrological cycle such as streamflow (Bachmair et al., 2016; Van Lanen et al., 2016). The real-time streamflow data provide fundamental measurements for drought forecasting based on hydrological model (e.g., Sutanto & Van Lanen, 2021) or observed flow (e.g., Modarres, 2007).

The RPR can extend the available methods of inexpensive measurements of river level and paves the way to real-time monitoring. RPR provides telemetry capabilities that can make data acquisition easier and more cost-effective, improving rapid response to flooding and drought events. The NMEA data can be processed on site in the RPR microcomputer instead of a data center. As such, the water level values can be transmitted to a data server (Figure 3c, *Option III*). Such analysis strategy allows to significantly reduce the amount of data being transmitted through GSM network or LoRaWAN radio network. Note that the current version of *gnssrefl* software (1.1.3) is not capable of real-time retrieval of water level as LSP methods requires about one hour data acquisition for a rising and setting satellite arc (with CPU time depending on the reflector height).

Although, with the advantages of affordable cost and low maintenance, RPR sensors have great potential to form a network of monitoring water level, the challenge of demonstrating plausibility of data from low-cost sensors in life-critical situations is still a concerning issue (Williams, 2019).

7 Summary and Concluding Remarks

With floods and droughts becoming increasingly frequent as climate change worsens, there is a compelling need to improve hydrological data collection. Inexpensive open-source hydrological sensors facilitate the acquisition of new *in-situ* data. In particular, inexpensive novel sensors are increasingly being developed for sea level and river water monitoring. We have developed a cost-effective water level sensor called Raspberry Pi Reflector (RPR), using Global Navigation Satellite System Interferometric Reflectometry (GNSS-IR). It has been demonstrated to be

capable of measuring river level with nearly centimeter level accuracy. Since the GNSS-IR instrument is not in contact with the water, it can be operated safely in extreme weather with lower operational costs. Our RPR sensor streams near real-time raw data allowing continuous water level measurement. Only a single-time site visit is required for installation. The device does not require any on-site calibration and involves only basic soldering and programing skills. The RPR consists of two main subsystems: (1) GNSS-IR sensor that includes single-frequency GPS receiver, microcontroller and external GPS antenna, and (2) Raspberry Pi microcomputer and cellular modem. We have been operating a unit on the Rhine river since March 2020 to examine the long-term performance of the RPR. The river level measurements from RPR were compared with co-located river gauge measurements. We obtained an overall accuracy of 3 cm for sub-daily water level measurement for the RPR setup with an antenna rotated 90 degrees from the vertical. The RPR does not need infrastructure such as a bridge or pier for installation, and it costs less than $150 U.S. dollars (as of November 2021). However, the RPR may not work well in narrow rivers (< ~ 50 m width) or in rivers located in steep valleys where satellite signals are blocked at low elevation angles. At our Wesel site, the unit successfully recorded flooding events associated with July 2021 flash rainfall event in western Europe and other heavy rainfall events. The successful deployment of the RPR over nearly two years showed its stability and durability. The RPR sensor can be applied to a variety of areas including rivers, lakes, dams and sea. It could aid stream flow estimation, and through pairs of devices along the river allows measuring river slope changes.

Acknowledgments

M. A. K. acknowledge partial funding from Austrian Science Fund (FWF) (project P30097-N29), The University of Bonn's Argelander Starter-Kit (project 36A-40003-27-71060007) and Deutsche Forschungsgemeinschaft (DFG) (project SFB 1502/1-2022, 450058266), F. G. N.: National Council for Scientific and Technological Development (CNPq; grant numbers 433099/2018-6 and 310752/2019-1) and the Rio Grande do Sul State Research Funding Agency (Fapergs, grant number 17/2551-0001127-9). K. M. L.: NASA (grant number 80NSSC20K1731). We thank Jan Böhme, the German Federal Waterways and Shipping Administration and Lutz Eberlein for logistical supports. We thank Yusuf Sermet and two anonymous reviewers, whose thoughtful comments improved the manuscript.

Open Research

RPR data processed in this study are available from https://doi.org/10.5281/zenodo.6828597.
The wind speed data are available from the German Weather Service (DWD) ftp server https://opendata.dwd.de/climate_environment/CDC/observations_germany/climate/hourly/wind/r

ecent). The last thirty day river gauge data in Wesel is available from the German Federal Waterways and Shipping Administration (WSV) web site (https://www.pegelonline.wsv.de/webservices/files/Wasserstand+Rohdaten/RHEIN/WESEL/). Access to the *gnssrefl* is available from https://doi.org/10.5281/zenodo.5601495. Guide to assemble a RPR sensor is provided in Supplement Information and in https://doi.org/10.5281/zenodo.6828562.

References

Adams J., Al Kaabi H., Brill S., Even R., Khan U., Miller M., Smith J., Whitney M. (2013) FROS-D: Free-Standing Receiver of Snow Depth (Aerospace Engineering Sciences Senior Design Project). University of Colorado Boulder, Department of Aerospace Engineering Sciences.

Adams III, T. E. (2016). Flood forecasting in the United States NOAA/national weather service. In Flood Forecasting: A Global Perspective, Academic Press, 249–310, https://doi.org/10.1016/B978-0-12-801884-2.00010-4.

NWS, (2010), Flood Warning Systems Manual. Accessed 27 September 2022, http://www.nws.noaa.gov/directives/010/archive/pd01009042c.pdf

Alonso-Arroyo, A., Camps, A., Park, H., Pascual, D., Onrubia, R., & Martín, F. (2014). Retrieval of significant wave height and mean sea surface level using the GNSS-R interference pattern technique: Results from a three-month field campaign. *IEEE Transactions on Geoscience and Remote Sensing*, *53*(6), 3198-3209.

Azevedo, J. A., & Brás, J. A. (2021). Measurement of Water Level in Urban Streams under Bad Weather Conditions. *Sensors*, *21*(21), 7157.

Bachmair, S., Stahl, K., Collins, K., Hannaford, J., Acreman, M., Svoboda, M., ... & Overton, I. C. (2016). Drought indicators revisited: the need for a wider consideration of environment and society. *Wiley Interdisciplinary Reviews: Water*, *3*(4), 516-536.

Beddows, P. A., & Mallon, E. K. (2018). Cave pearl data logger: A flexible Arduino-based logging platform for long-term monitoring in harsh environments. *Sensors*, *18*(2), 530.

Biancamaria, S., Lettenmaier, D. P., & Pavelsky, T. M. (2016). The SWOT mission and its capabilities for land hydrology. In *Remote sensing and water resources* (pp. 117-147). Springer, Cham.

Boon, J. D., & Brubaker, J. M. (2008, September). Acoustic-microwave water level sensor comparisons in an estuarine environment. In *OCEANS 2008* (pp. 1-5). IEEE.

Chandler, J., Ashmore, P., Paola, C., Gooch, M., & Varkaris, F. (2002). Monitoring river-channel change using terrestrial oblique digital imagery and automated digital photogrammetry. *Annals of the Association of American Geographers*, *92*(4), 631-644.

Chen, G., Bai, K., Lin, Z., Liao, X., Liu, S., Lin, Z., ... & Jia, X. (2021). Method on water level ruler reading recognition based on image processing. *Signal, Image and Video Processing*, *15*(1), 33-41.

Costa, J. E., Cheng, R. T., Haeni, F. P., Melcher, N., Spicer, K. R., Hayes, E., ... & Barrick, D. (2006). Use of radars to monitor stream discharge by noncontact methods. *Water Resources Research*, *42*(7).

Eltner, A., Elias, M., Sardemann, H., & Spieler, D. (2018). Automatic image-based water stage measurement for long-term observations in ungauged catchments. *Water Resources*

Research, *54*(12), 10-362.Escudier, P., Couhert, A., Mercier, F., Mallet, A., Thibaut, P., Tran, N., ... & Dorandeu, J. (2017). Satellite Radar Altimetry: Principle, Accuracy, and Precision. In *Satellite altimetry over oceans and land surfaces* (pp. 1-70). CRC Press.

Fagundes, M. A. R., Mendonça-Tinti, I., Iescheck, A. L., Akos, D. M., & Geremia-Nievinski, F. (2021). An open-source low-cost sensor for SNR-based GNSS reflectometry: design and long-term validation towards sea-level altimetry. *GPS Solutions*, *25*(2), 1-11.

Franchini, M., & Lamberti, P. (1994). A flood routing Muskingum type simulation and forecasting model based on level data alone. *Water resources research*, *30*(7), 2183-2196.

Geremia-Nievinski, F., Hobiger, T., Haas, R., Liu, W., Strandberg, J., Tabibi, S., Vey, S., Wickert, J., & Williams, S. (2020). SNR-based GNSS reflectometry for coastal sea-level altimetry: Results from the first IAG inter-comparison campaign. *Journal of Geodesy*, 94(8), 70.

Gill, S. K., and T. N. Mero. 1990. Next generation water level measurement system: Implementation into the NOAA National Water Level Observation Network. In Towards an integrated system for measuring long term changes in global sea level, ed. H. F. Eden, Report of a workshop held at Woods Hole Oceanographic Institution, May 1990, pp. 133-146. Washington, DC: Joint Oceanographic Institutions Inc. (JOI).

Gurtner, W., & Estey, L. (2007a). RINEX: The receiver independent exchange format version 2.11.

Gurtner, W., & Estey, L. (2007b). Rinex-the receiver independent exchange format-version 3.00. *Astronomical Institute, University of Bern and UNAVCO, Bolulder, Colorado.*

Hannah, D. M., Demuth, S., van Lanen, H. A., Looser, U., Prudhomme, C., Rees, G., ... & Tallaksen, L. M. (2011). Large-scale river flow archives: importance, current status and future needs. *Hydrological Processes*, *25*(7), 1191-1200.

Holden, L. D., & Larson, K. M. (2021). Ten years of Lake Taupō surface height estimates using the GNSS interferometric reflectometry. *Journal of Geodesy*, *95*(7), 1-12.

IOC. (2006). *Manual on sea level measurement and interpretation, volume IV: an update to 2006* (IOC Manuals and Guides No.14, vol. IV; JCOMM Technical Report No. 31; WMO/TD. No. 1339; p. 78). Intergovernmental Oceanographic Commission of UNESCO.

Jafarzadegan, K., Muñoz, D. F., Moftakhari, H., Gutenson, J. L., Savant, G., & Moradkhani, H. (2022). Real-time coastal flood hazard assessment using DEM-based hydrogeomorphic classifiers. *Natural Hazards and Earth System Sciences*, *22*(4), 1419-1435.

Jarihani, A. A., Callow, J. N., Johansen, K., & Gouweleeuw, B. (2013). Evaluation of multiple satellite altimetry data for studying inland water bodies and river floods. *Journal of Hydrology*, *505*, 78-90.

Karegar, M. A., & Kusche, J. (2020). Imprints of COVID-19 lockdown on GNSS observations: An initial demonstration using GNSS interferometric reflectometry. *Geophysical research letters*, *47*(19), e2020GL089647.

Khin, J. M. M., & Oo, N. N. (2018). Real-time vehicle tracking system using Arduino, GPS, GSM and web-based technologies. *International Journal of Science and Engineering Applications*, *7*(11,433-436).

Kim, J., Han, Y., & Hahn, H. (2011). Embedded implementation of image-based water-level measurement system. *IET computer vision*, *5*(2), 125-133.

Knight, P. J., Bird, C. O., Sinclair, A., & Plater, A. J. (2020). A low-cost GNSS buoy platform for measuring coastal sea levels. *Ocean Engineering*, *203*, 107198.

Knight, P., Bird, C., Sinclair, A., Higham, J., & Plater, A. (2021). Testing an "IoT" Tide Gauge Network for Coastal Monitoring. *IoT*, *2*(1), 17-32.

Krzysztofowicz, R. (2002). Bayesian system for probabilistic river stage forecasting. *Journal of hydrology*, *268*(1-4), 16-40.

Kuo, L. C., & Tai, C. C. (2022). Robust Image-Based Water-Level Estimation Using Single-Camera Monitoring. *IEEE Transactions on Instrumentation and Measurement*, *71*, 1-11.

Larson, K. M. (2021). kristinemlarson/gnssrefl: First release (1.0.10). Zenodo. https://doi.org/10.5281/zenodo.5601495

Larson, K. M., & Nievinski, F. G. (2013). GPS snow sensing: results from the EarthScope Plate Boundary Observatory. *GPS solutions*, *17*(1), 41-52.

Larson, K. M., Braun, J. J., Small, E. E., Zavorotny, V. U., Gutmann, E. D., & Bilich, A. L. (2009). GPS multipath and its relation to near-surface soil moisture content. *IEEE Journal of Selected Topics in Applied Earth Observations and Remote Sensing*, *3*(1), 91-99.

Larson, K. M., Löfgren, J. S., & Haas, R. (2013b). Coastal sea level measurements using a single geodetic GPS receiver. *Advances in Space Research*, *51*(8), 1301-1310.

Larson, K. M., Ray, R. D., Nievinski, F. G., & Freymueller, J. T. (2013a). The accidental tide gauge: a GPS reflection case study from Kachemak Bay, Alaska. *IEEE Geoscience and Remote Sensing Letters*, *10*(5), 1200-1204.

Leduc, P., Ashmore, P., & Sjogren, D. (2018). Stage and water width measurement of a mountain stream using a simple time-lapse camera. *Hydrology and Earth System Sciences*, *22*(1), 1-11.

Li, D., Fang, Z. N., & Bedient, P. B. (2021). Flood early warning systems under changing climate and extreme events. In *Climate Change and Extreme Events* (pp. 83-103). Elsevier.

Li, W., Liao, Q., & Ran, Q. (2019). Stereo-imaging LSPIV (SI-LSPIV) for 3D water surface reconstruction and discharge measurement in mountain river flows. *Journal of Hydrology*, *578*, 124099.

Liechti, C. (2020). PySerial documentation. Version 3.4, Copyright 2021-2020, Available under the BSD-3-Clause license: https://pyserial.readthedocs.io/en/latest/appendix.html#license

Lin, Y. T., Lin, Y. C., & Han, J. Y. (2018). Automatic water-level detection using single-camera images with varied poses. *Measurement*, *127*, 167-174.

Löfgren, J. S., Haas, R., & Scherneck, H. G. (2014). Sea level time series and ocean tide analysis from multipath signals at five GPS sites in different parts of the world. *Journal of Geodynamics*, *80*, 66-80.

Lomb, N. R. (1976). Least-squares frequency analysis of unequally spaced data. *Astrophysics and space science*, *39*(2), 447-462.

Lora Alliance. (2017). LoRaWAN 1.1 Specification. https://lora-alliance.org/resource_hub/lorawan-specification-v1-1/

Lyman, T. P., Elsmore, K., Gaylord, B., Byrnes, J. E., & Miller, L. P. (2020). Open Wave Height Logger: An open source pressure sensor data logger for wave measurement. *Limnology and Oceanography: Methods*, *18*(7), 335-345.

Mao, F., Khamis, K., Clark, J., Krause, S., Buytaert, W., Ochoa-Tocachi, B. F., & Hannah, D. M. (2020). Moving beyond the technology: a socio-technical roadmap for low-cost water sensor network applications. *Environmental Science & Technology*, *54*(15), 9145-9158.

Martin, C. R., Zeng, N., Karion, A., Dickerson, R. R., Ren, X., Turpie, B. N., & Weber, K. J. (2017). Evaluation and environmental correction of ambient CO 2 measurements from a low-cost NDIR sensor. *Atmospheric measurement techniques*, *10*(7), 2383-2395.

Modarres, R. (2007). Streamflow drought time series forecasting. *Stochastic Environmental Research and Risk Assessment*, *21*(3), 223-233.

Muhadi, N. A., Abdullah, A. F., Bejo, S. K., Mahadi, M. R., & Mijic, A. (2021). Deep Learning Semantic Segmentation for Water Level Estimation Using Surveillance Camera. *Applied Sciences*, *11*(20), 9691.

Nievinski, F. G., & Larson, K. M. (2014). Forward modeling of GPS multipath for near-surface reflectometry and positioning applications. *GPS solutions*, *18*(2), 309-322.

NMEA. (2018). *NMEA 0183 Interface Standard (Version 4.11).* National Marine Electronics Association. https://www.nmea.org/content/STANDARDS/NMEA_0183_Standard

Noye, B. J. 1974. Tide-well systems I: Some non-linear effects of the conventional tide well. J. Mar. Res. 32(2): 129-135.

Paul, J. D., Buytaert, W., & Sah, N. (2020). A technical evaluation of lidar-based measurement of river water levels. *Water Resources Research*, *56*(4), e2019WR026810.

Penna, N. T., Morales Maqueda, M. A., Martin, I., Guo, J., & Foden, P. R. (2018). Sea surface height measurement using a GNSS Wave Glider. *Geophysical Research Letters*, 45, 5609–5616.

Perera, D., Seidou, O., Agnihotri, J., Rasmy, M., Smakhtin, V., Coulibaly, P., & Mehmood, H. (2019). Flood early warning systems: a review of benefits, challenges and prospects. *UNU-INWEH, Hamilton*.

Princy, S. E., & Nigel, K. G. J. (2015, November). Implementation of cloud server for real time data storage using Raspberry Pi. In *2015 Online International Conference on Green Engineering and Technologies (IC-GET)* (pp. 1-4). IEEE.

Pugh, D. T. 1972. The physics of pneumatic tide gauges. Int. Hydrogr. Rev. 49(2): 71-97.

Purnell, D. J., Gomez, N., Minarik, W., Porter, D., & Langston, G. (2021). Precise water level measurements using low-cost GNSS antenna arrays. *Earth Surface Dynamics*, *9*(3), 673-685.

Reid, A. J., Carlson, A. K., Creed, I. F., Eliason, E. J., Gell, P. A., Johnson, P. T., ... & Cooke, S. J. (2019). Emerging threats and persistent conservation challenges for freshwater biodiversity. *Biological Reviews*, *94*(3), 849-873.

Reinking, J., Roggenbuck, O., & Even-Tzur, G. (2019). Estimating wave direction using terrestrial GNSS reflectometry. *Remote Sensing*, *11*(9), 1027.

Rizos, C., & Han, S. (2003). Reference station network based RTK systems-concepts and progress. *Wuhan University Journal of Natural Sciences*, *8*(2), 566-574.

Rodrigues, F. S., & Moraes, A. O. (2019). ScintPi: A low-cost, easy-to-build GPS ionospheric scintillation monitor for DASI studies of space weather, education, and citizen science initiatives. *Earth and Space Science*, *6*(8), 1547-1560.

Roesler, C., & Larson, K. M. (2018). Software tools for GNSS interferometric reflectometry (GNSS-IR). *GPS solutions*, *22*(3), 1-10.

Roggenbuck, O., & Reinking, J. (2019). Sea surface heights retrieval from ship-based measurements assisted by GNSS signal reflections. *Marine Geodesy*, *42*(1), 1-24.

Roussel, N., Ramillien, G., Frappart, F., Darrozes, J., Gay, A., Biancale, R., ... & Allain, D. (2015). Sea level monitoring and sea state estimate using a single geodetic receiver. *Remote sensing of Environment*, *171*, 261-277.

Ruhi, A., Messager, M. L., & Olden, J. D. (2018). Tracking the pulse of the Earth's fresh waters. *Nature Sustainability*, *1*(4), 198-203.

Ruhi, A., Olden, J. D., & Sabo, J. L. (2016). Declining streamflow induces collapse and replacement of native fish in the American Southwest. *Frontiers in Ecology and the Environment*, *14*(9), 465-472.

Sanders, W., Li, D., Li, W., & Fang, Z. N. (2022). Data-Driven Flood Alert System (FAS) Using Extreme Gradient Boosting (XGBoost) to Forecast Flood Stages. *Water*, *14*(5), 747.

Santamaría-Gómez, A., & Watson, C. (2017). Remote leveling of tide gauges using GNSS reflectometry: case study at Spring Bay, Australia. *GPS solutions*, *21*(2), 451-459.

Scargle, J. D. (1982). Studies in astronomical time series analysis. II-Statistical aspects of spectral analysis of unevenly spaced data. *The Astrophysical Journal*, *263*, 835-853.

Sermet, Y., & Demir, I. (2022). Camera-Based Intelligent Stream Stage Sensing for Decentralized Environmental Monitoring.

Smith, P. J., Pappenberger, F., Wetterhall, F., Del Pozo, J. T., Krzeminski, B., Salamon, P., ... & Baugh, C. (2016). On the operational implementation of the European Flood Awareness System (EFAS). In *Flood forecasting* (pp. 313-348). Academic Press.

Strandberg, J., Hobiger, T., & Haas, R. (2016). Improving GNSS-R sea level determination through inverse modeling of SNR data. *Radio Science*, *51*(8), 1286-1296.

Strandberg, J., Hobiger, T., & Haas, R. (2019). Real-time sea-level monitoring using Kalman filtering of GNSS-R data. *GPS Solutions*, *23*(3), 1-12.

Sutanto, S. J., & Van Lanen, H. A. (2021). Streamflow drought: implication of drought definitions and its application for drought forecasting. *Hydrology and Earth System Sciences*, *25*(7), 3991-4023.

Townsend, K. (2022). Introducing the Adafruit WICED Feather, Online available at: https://cdn-learn.adafruit.com/downloads/pdf/introducing-the-adafruit-wiced-feather-wifi.pdf

Tuozzolo, S., Lind, G., Overstreet, B., Mangano, J., Fonstad, M., Hagemann, M., ... & Durand, M. (2019). Estimating river discharge with swath altimetry: A proof of concept using AirSWOT observations. *Geophysical Research Letters*, *46*(3), 1459-1466.

UNDRR: Terminology for Disaster Risk Reduction, UNDRR, Geneva, Switzerland, https://www.undrr.org/terminology (last access: 07 June 2022), 2017.

Upton, E., & Halfacree, G. (2014). *Raspberry Pi user guide*. John Wiley & Sons.

Van Lanen, H. A., Laaha, G., Kingston, D. G., Gauster, T., Ionita, M., Vidal, J. P., ... & Van Loon, A. F. (2016). Hydrology needed to manage droughts: the 2015 European case. *Hydrological Processes*, *30*(17), 3097-3104.

Vandaele, R., Dance, S. L., & Ojha, V. (2021). Deep learning for automated river-level monitoring through river-camera images: An approach based on water segmentation and transfer learning. *Hydrology and Earth System Sciences*, *25*(8), 4435-4453.

Vanden Boomen, R. L., Yu, Z., & Liao, Q. (2021). Application of Deep Learning for Imaging-Based Stream Gaging. *Water Resources Research*, *57*(11), e2021WR029980.

VanderPlas, J. T. (2018). Understanding the lomb–scargle periodogram. *The Astrophysical Journal Supplement Series*, *236*(1), 16.

Vieux, B. E., Cui, Z., & Gaur, A. (2004). Evaluation of a physics-based distributed hydrologic model for flood forecasting. *Journal of hydrology*, *298*(1-4), 155-177.

Williams, S. D., Bell, P. S., McCann, D. L., Cooke, R., & Sams, C. (2020). Demonstrating the potential of low-cost GPS units for the remote measurement of tides and water levels using interferometric reflectometry. *Journal of Atmospheric and Oceanic Technology*, *37*(10), 1925-1935.

Williams, D. E. (2019). Low cost sensor networks: how do we know the data are reliable?. ACS sensors, 4(10), 2558-2565.

Woodworth, P. L., & Smith, D. E. (2003). A one year comparison of radar and bubbler tide gauges at Liverpool. *The International hydrographic review*.

Yaseen, Z. M., El-Shafie, A., Jaafar, O., Afan, H. A., & Sayl, K. N. (2015). Artificial intelligence based models for stream-flow forecasting: 2000–2015. *Journal of Hydrology*, *530*, 829-844.

Young, D. S., Hart, J. K., & Martinez, K. (2015). Image analysis techniques to estimate river discharge using time-lapse cameras in remote locations. *Computers & geosciences*, *76*, 1-10.

Zhang, Z., Zhou, Y., Liu, H., & Gao, H. (2019). In-situ water level measurement using NIR-imaging video camera. *Flow Measurement and Instrumentation*, *67*, 95-106.